THE JOURNAL OF PHYSICAL CHEMISTRY C
A JOURNAL OF THE AMERICAN CHEMICAL SOCIETY

pubs.acs.org/JPCC

Article

# Mechanical, Electronic, and Optical Properties of 8-16-4 Graphyne: A 2D Carbon Allotrope with Dirac Cones

Raphael M. Tromer, Marcelo L. Pereira Júnior, Kleuton A. L. Lima, Alexandre F. Fonseca, Luciano R. da Silva, Douglas S. Galvão, and Luiz. A. Ribeiro Junior*

Cite This: J. Phys. Chem. C 2023, 127, 12226−12234

Read Online

ACCESS | Metrics & More | Article Recommendations | Supporting Information

**ABSTRACT:** Graphene's success has led to the theoretical prediction and experimental synthesis of various 2D carbon-based allotropes. To explore the mechanical, structural, electronic, and optical properties of 8-16-4 graphyne, we employed density functional theory using the GGA/PBE approach, ab initio molecular dynamics (AIMD), and classical reactive molecular dynamics simulations. Our AIMD results indicate that this material demonstrates excellent dynamical and thermal stabilities. It has a formation energy of −8.57 eV/atom and an elastic moduli of 262.37 GPa. Regarding its band structure, this graphyne analogue is a semimetal with two Dirac cones. It also exhibits transparency and intense optical activity in the infrared region. Notably, the band structure of 8-16-4 graphyne remains practically unchanged at moderate strain regimes. To our knowledge, this is the first known 2D carbon allotrope to exhibit such behavior.

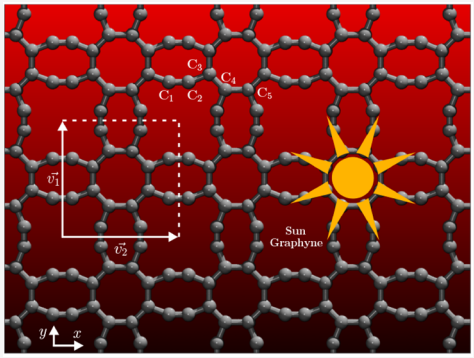


## INTRODUCTION

Since the discovery of graphene in 2004,[1] there has been a renewed interest in 2D carbon materials.[2−5] Depending on the synthesis process, they exhibit controllable physicochemical properties.[6,7] Several 2D carbon allotropes have been proposed,[8−18] and a few of them have been already experimentally realized.[19−22] Among the recently synthesized structures, it is worth mentioning monolayer amorphous carbon (MAC),[19] 2D biphenylene network (BPN),[20] monolayer fullerene network ($2DC_{60}$),[22] and the multilayer γ-graphyne.[21]

MAC and BPN share some properties with graphene, such as a zero semimetal bandgap and Dirac cones exhibiting linear dispersion. However, MAC possesses randomly distributed defects involving five, six, seven, and eight carbon atom rings. This results in a distinct lattice arrangement compared to disordered graphene. On the other hand, the BPN lattice exhibits a periodic arrangement of carbon rings with four, six, and eight atoms. In contrast, γ-graphyne and $2DC_{60}$ exhibit a small direct bandgap of 0.48 eV[21] and a direct semiconducting bandgap of 1.6 eV,[22] respectively.

"Graphynes" encompasses structures where acetylene groups are inserted into single bonds. The lattice structure of γ-graphyne can be visualized as graphene expanded uniformly by incorporating two-carbon acetylenic units between all the aromatic rings. The prediction of graphyne structures dates back to 1987[23]. Within this category, there are graphyne-based molecules known as fullereneynes,[24] as well as graphyne-based nanotubes[25] and nanoscrolls,[26] which have been extensively documented in the literature.

2DC60 crystals are created through the covalent bonding of C60 polymers, forming a planar configuration. This clustering process forms two stable crystals with closely packed quasi-hexagonal and quasi-tetragonal phases.[22] Both γ-graphyne and $2DC_{60}$ address the challenge of lacking a bandgap, which restricts the usability of other 2D carbon-based materials in digital electronics applications.

There have been proposals for carbon-based materials, as well as materials composed of different atomic species, that exhibit Dirac cones.[9,27−30] Examples include S-graphene[31] and 6,6,12-graphyne,[32] which can feature an additional Dirac point in their band structure profiles. An external strain applied to these materials allows for manipulating the Dirac point. The two Dirac cones merge in moderate strain regimes into a single cone. When subjected to high strain rates, a transition from semimetallic to semiconductor behavior occurs, resulting in the disappearance of the Dirac cones and the opening of a bandgap.

Preserving optoelectronic properties under external stress is desirable for applications in flexible electronics. Surprisingly, no discussion regarding a 2D carbon-based material exhibiting this property is presented in the literature. Therefore, the primary objective of this study is to address this research gap

Received: March 16, 2023
Revised: May 18, 2023
Published: June 16, 2023

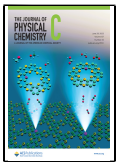

and provide insights into a material that maintains its optoelectronic properties even when subjected to external stress.

This study explores the mechanical, structural, electronic, and optical properties of 8-16-4 graphyne,[33] a 2D carbon-based material known for its distinctive band structure featuring two Dirac cones. For the sake of simplicity, we will refer to it as Sun-Graphyne (S-GY) throughout this paper (see Figure 1).

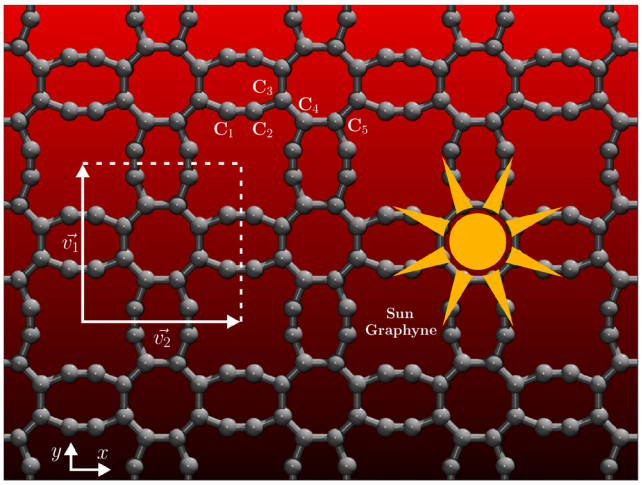


**Figure 1.** Schematic representation of the S-GY structure. The square highlights the symmetric unit cell. The unit cell vectors are $|\vec{v}_1| = |\vec{v}_2| =$ 7.36 Å.

The name "Sun-Graphyne" is chosen due to its lattice structure, which is similar to other graphyne variants, and its unit cell arrangement resembling the shape of a sun drawing.[23,34,35] To investigate the electronic, mechanical, and optical properties of S-GY, we employed density functional theory (DFT), as well as *ab initio* and classical molecular dynamics (MD) methods. Importantly, 2D systems of similar complexity have recently been successfully addressed using AIMD simulations.[36−38] Our comprehensive analysis demonstrates the thermal stability of S-GY even at elevated temperatures.

The structure of S-GY belongs to a class of graphyne structures that were designed theoretically. Our starting point was octa-graphene,[39] and we introduced acetylene groups into the bonds of the square octa-graphene rings. It is important to note that S-GY differs from another type of graphyne called T-graphyne (also known as octa-graphyne),[40,41] which consists of a single eight-atom ring. What sets S-GY apart from other Dirac materials is that its electronic band structure remains relatively unchanged under moderate strain conditions.

## METHODOLOGY

**DFT Calculations.** DFT simulations were employed to investigate S-GY's electronic and optical properties. These simulations were performed using the SIESTA code,[42] within the framework of the generalized gradient approximation (GGA) with the Perdew−Burke−Ernzenhof (PBE) exchange-correlation functional.[43,44]

Norm-conserving Troullier−Martins pseudopotentials[45] were used to accurately describe the core electrons in the calculations. The computations also incorporated van der Waals (vdw-DFT) corrections to account for the dispersion forces.[46−48] The basis set employed was double-$\zeta$ plus polarization (DZP). A vacuum region of 20 Å was included to prevent unwanted interactions between periodic images. A kinetic energy cutoff value of 300 eV was chosen. A k-grid of 10 × 10 × 1 was used for geometry optimizations, while electronic and optical calculations used a denser k-grid of 30 × 30 × 1.

In our simulations, we employed the ab initio molecular dynamics (AIMD) approach to accurately account for S-GY's thermal stability at finite temperatures. To maintain a constant temperature once equilibrium was achieved, we employed a Nosé−Hoover thermostat.[49] The simulations were conducted using an NVT ensemble with a time step of 1.0 fs, allowing us to explore the system's dynamics over a total simulation time of 2 ps.

For the optical calculations, a standard external electric field of 1.0 V/Å was applied along the *x*-, *y*-, and *z*-directions.[50] Using the Kramers−Kronig relation and Fermi's golden rule, we could determine the dielectric constant's real part ($\epsilon_1$) and imaginary part ($\epsilon_2$):

$$\epsilon_1(\omega) = 1 + \frac{1}{\pi} P \int_0^\infty d\omega' \frac{\omega' \epsilon_2(\omega')}{\omega'^2 - \omega^2} \tag{1}$$

where $P$ is the Cauchy principal value, and

$$\epsilon_2(\omega) = \frac{4\pi^2}{V_\Omega \omega^2} \sum_{i \in VB, j \in CB} \sum_k W_k |\rho_{ij}|^2 \delta(\varepsilon_{kj} - \varepsilon_{ki} - \hbar\omega) \tag{2}$$

where $W_k$ is the $k$-point weight in the reciprocal space, $\rho_{ij}$ the dipole transition matrix element, $\hbar\omega$ the photon frequency, and $V_\Omega$ the unit cell volume. VB and CB denote the valence and conduction bands, respectively.[16]

Once the real and imaginary parts of the dielectric constant are determined, it becomes possible to calculate other critical optical coefficients. These include the absorption coefficient ($\alpha$), the refractive index ($\eta$), and the reflectivity ($R$):

$$\alpha(\omega) = \sqrt{2}\,\omega[(\epsilon_1^2(\omega) + \epsilon_2^2(\omega))^{1/2} - \epsilon_1(\omega)]^{1/2} \tag{3}$$

$$\eta(\omega) = \frac{1}{\sqrt{2}}[(\epsilon_1^2(\omega) + \epsilon_2^2(\omega))^{1/2} + \epsilon_1(\omega)]^2 \tag{4}$$

and

$$R(\omega) = \left[\frac{(\epsilon_1(\omega) + i\epsilon_2(\omega))^{1/2} - 1}{(\epsilon_1(\omega) + i\epsilon_2(\omega))^{1/2} + 1}\right]^2 \tag{5}$$

**Classical MD Simulations.** Classical reactive MD simulations were conducted to explore the fracture patterns, dynamics, and thermal stability of S-GY. These simulations provided a detailed understanding of the system's dynamic behavior. The Large-scale Atomic/Molecular Massively Parallel Simulator (LAMMPS) code[51,52] was used for performing these fully atomistic MD simulations. A reactive force field was necessary because fracture involves bond breakage and formation. Consequently, we employed the Adaptive Intermolecular Reactive Empirical Bond Order Potential (AIREBO)[53] to accurately capture the bond dynamics during the simulations.

To solve Newton's equations of motion, we employed the Velocity-Verlet Algorithm. The integration time step was set to 0.1 fs, and we used an NPT ensemble with the Nosé−Hoover thermostat to maintain a constant temperature.[54] The





https://doi.org/10.1021/acs.jpcc.3c01788
J. Phys. Chem. C 2023, 127, 12226−12234

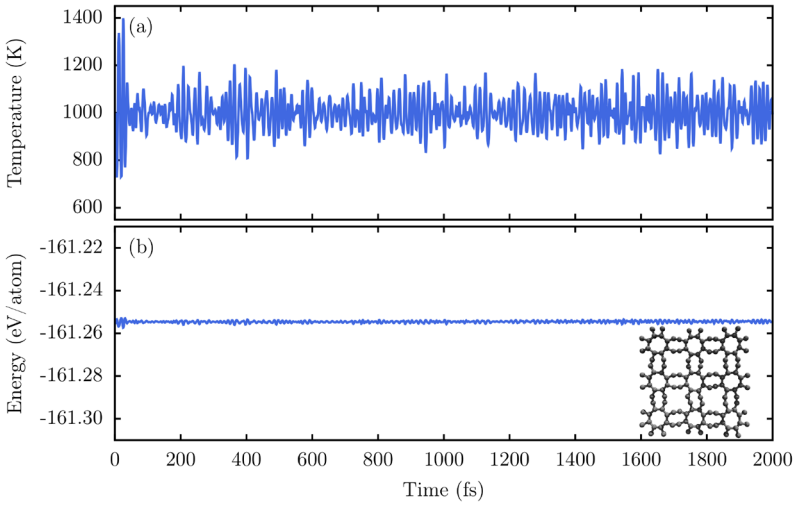


**Figure 2.** System's time evolution is depicted in parts (a) and (b), showcasing the temperature and potential energy per atom, respectively. The final configuration of S-GY is captured in the representative AIMD snapshot in panel (b). The simulation encompassed a total time of 2 ps, maintaining a temperature of 1000 K.

simulations encompassed a temperature range from room temperature up to 7000 K while maintaining null pressure. Before the main simulations, an equilibration period of 200 ps was performed to eliminate residual stress within the S-GY lattice.

The systems analyzed in this study had an approximate area of 104 $nm^2$, encompassing a 14 × 14 × 1 unit cell (comprising 3136 atoms) with periodic boundary conditions. The unit cell, highlighted in Figure 1, contained 16 carbon atoms. A lattice constant of 100 Å (vacuum buffer zone) was employed along the *z*-direction to prevent any interaction between S-GY and its periodic images.

In the strain simulations, we focused solely on the *x*-direction as it suffices to account for the symmetry of the S-GY unit cell (refer to Figure 1). To induce strain, we increased the size of the simulation box with a constant uniaxial strain rate of $10^{-6}$ $fs^{-1}$ at room temperature. This simulation protocol allowed us to generate stress−strain curves and determine the material's elastic properties by examining representative MD snapshots. We could analyze the fracture patterns and dynamic behavior of the system.

We employed a heating ramp protocol to assess the thermal stability of S-GY. The temperature was systematically raised from room temperature to 7000 K at a constant rate of 2 K/ps. These simulations were performed under the NVT ensemble for 1 ns. By analyzing the resulting data, we could estimate the melting point of S-GY. We utilized the software VMD to visualize and analyze the MD snapshots and trajectories.[55]

## RESULTS

**Stability and Structural Properties.** Figure 1 illustrates the optimized lattice structure of S-GY, with its symmetric unit cell highlighted within a square. The unit cell vectors have lengths of $|\vec{v}_1| = |\vec{v}_2| = 7.36$ Å. S-GY is composed entirely of carbon atoms, arranged periodically, featuring two distinct eight-atom rings. The bond lengths within these rings are $\overline{C_1C_2} = 1.24$ Å and $\overline{C_2C_3} = 1.42$ Å for one ring, and $\overline{C_3C_4} = 1.42$ Å and $\overline{C_4C_5} = 1.48$ Å for the other ring, as depicted in Figure 1. These bond length values are consistent with those observed in similar 2D carbon allotropes.[56,57] Notably, the formation energy of S-GY is −8.57 eV/atom, which closely resembles that of graphene (−8.8 eV/atom).[50,58,59]

AIMD simulations were conducted to assess the structural stability of S-GY for a duration of 2 ps at a temperature of 1000 K. Figures 2a and 2b depict the system's time evolution, showcasing the temperature and potential energy per atom, respectively. Figure 2a also presents the representative AIMD snapshot at the simulation's conclusion. The figure reveals that the S-GY structure remains unaltered even under high-temperature conditions, with minor deviations observed (such as slight tilting of some rings) due to thermal fluctuations. The calculated formation energy and AIMD result collectively indicate the good structural stability of S-GY. Furthermore, recent advancements in graphyne syntheses[35,60,61] suggest the possibility of synthesizing S-GY.

**Electronic Properties.** Figure 3 showcases the electronic band structure of S-GY in various conditions: unstrained (3a) and under biaxial strain (5% strain in 3b and 10% strain in 3c). A notable observation is two Dirac points along the X → M and M → Y integration paths, indicating the S-GY electrons' resemblance to massless Dirac fermions, much like graphene. These Dirac points are separated by a narrow gap of approximately 5 meV. Additionally, the symmetry of S-GY is evident in the isotropic transport channels observed along the M → Γ or M ← Γ directions.

The electronic band structure of S-GY, as depicted in Figures 3a and 3b, exhibits remarkable stability even under moderate strain conditions. Unlike other 2D carbon-based materials with Dirac cones, no symmetry inversion is observed. Figures 3b and 3c illustrate the S-GY band structure under biaxial strains of 5% and 10%, respectively. Interestingly, both configurations resemble the unstrained case. In contrast, other graphyne materials can exhibit tunable band structures under applied stress.[32] For instance, at a biaxial strain of 6%, the two Dirac cones merge into a single cone,[32] while a bandgap emerges at an 8% strain.[32] This result differs from our findings, where the S-GY's Dirac cone remains stable even at higher strain values.

In addition to the band structure calculations at the GGA/PBE level, we have also conducted calculations for unstrained


https://doi.org/10.1021/acs.jpcc.3c01788
J. Phys. Chem. C 2023, 127, 12226−12234

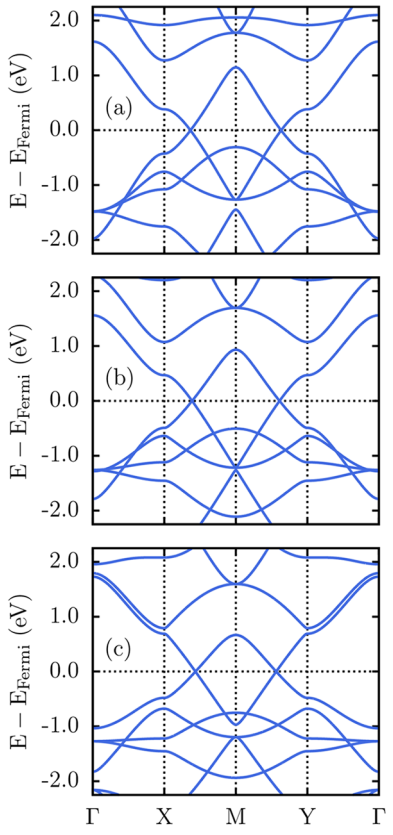


**Figure 3.** S-GY electronic band structure for the unstrained (a) and with (b) 5% and (c) 10% of applied biaxial strain.

S-GY using the HSE06 method (see the Supporting Information). The results obtained from the HSE06 calculations exhibit a similar band structure configuration to that of the GGA/PBE calculations. Expressly, the HSE06 calculations confirm the presence of two Dirac cones in S-GY without indicating a gap opening in the material.

To gain further insights into the band configuration of S-GY, we analyzed the impact of bilayer interactions on its electronic properties, as depicted in Figure 4. It is evident from this figure that the prominent electronic characteristics resemble those observed in the monolayer case but with the addition of two extra Dirac cones. These additional cones signify the contribution of the extra layer to the overall electronic properties of S-GY.

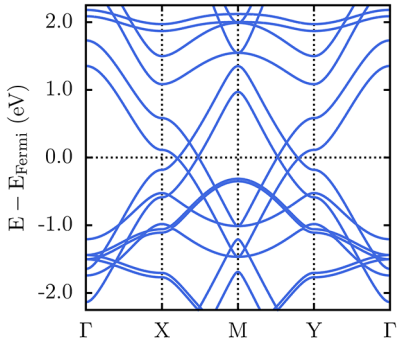


**Figure 4.** Electronic band structure configuration for the S-GY bilayer.

**Optical Properties.** Figure 5 illustrates the variation of optical coefficients with photon energy in the 0−20 eV range

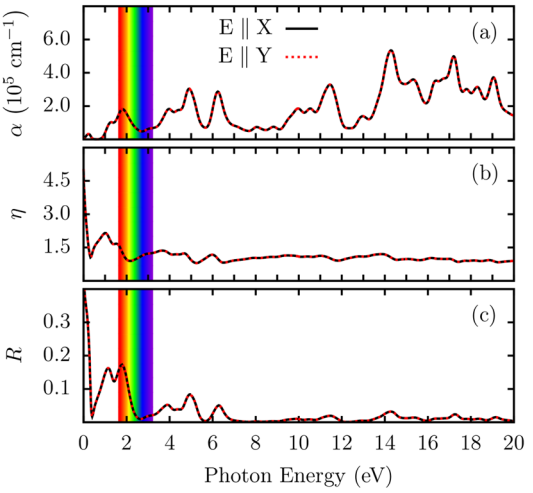


**Figure 5.** (a) Absorption coefficient, (b) refractive index, and (c) reflectivity as a function of photon energy for the S-GY monolayer. $E\|X$ and $E\|Y$ denote the polarization direction for the externally applied electric field.

under an external electric field polarized along the $x$- and $y$-directions. The absorption spectrum (Figure 5a) begins near 0 eV, primarily attributed to $\pi$ to $\pi^*$ transitions, as inferred from the density of states (see the Supporting Information). This behavior aligns with the semimetallic nature of S-GY, possessing a small electronic bandgap of 5 meV, as previously mentioned. Notably, several absorption peaks span from the infrared to ultraviolet regions. The maximum intensity of absorption reaches approximately $3 \times 10^5$ cm$^{-1}$ for photon energies up to 12 eV, which subsequently increases to $5 \times 10^5$ cm$^{-1}$ for higher photon energies. Notably, a single peak emerges within the visible region at 1.9 eV. Moreover, the isotropic optical properties along the $x$- and $y$-directions are observed in S-GY, aligning with its topological characteristics.

Figure 5b displays the refractive index, where the exception is its value at zero photon energy. The peak intensity corresponds to the 1 eV peak, while $\eta$ exhibits a slight decrease at 2 eV, remaining nearly constant across the remaining spectra. Similarly, Figure 5c demonstrates the reflectivity of S-GY, with the maximum intensity observed between 1 and 2 eV. The reflectivity activity is confined to the infrared region and diminishes to values close to zero for photon energies exceeding 3 eV. These findings suggest that incident light on S-GY is predominantly absorbed, indicating its transparency as a material.

The optical analysis was also conducted for the bilayer configuration, and as anticipated, there are no significant distinctions in the optical activity compared to the monolayer case, as depicted in Figure 6. However, the bilayer configuration exhibits higher light absorption values, reaching approximately $8 \times 10^5$ cm$^{-1}$ (see Figure 6a). The behavior of $R$ and $\eta$ is similar between the two systems (see Figures 6b and 6c, respectively), except for null photon energy.

We examined the spatial patterns of the frontier crystalline orbitals, specifically the lowest unoccupied crystalline orbital (LUCO) and the highest occupied crystalline orbital (HOCO). These results are illustrated in Figures 7a and 7b,



https://doi.org/10.1021/acs.jpcc.3c01788
J. Phys. Chem. C 2023, 127, 12226−12234

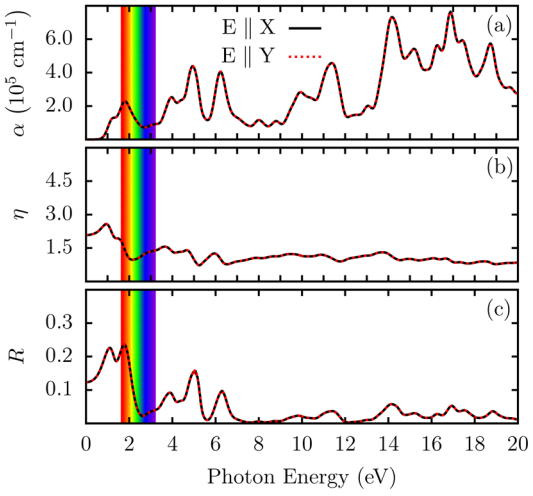


**Figure 6.** (a) Absorption coefficient, (b) refractive index, and (c) reflectivity as a function of photon energy for the S-GY bilayer. $E\|X$ and $E\|Y$ denote the polarization direction for the externally applied electric field.

respectively. Both crystalline orbitals extend across the lattice, indicating electronic delocalization and corroborating the small bandgap value.

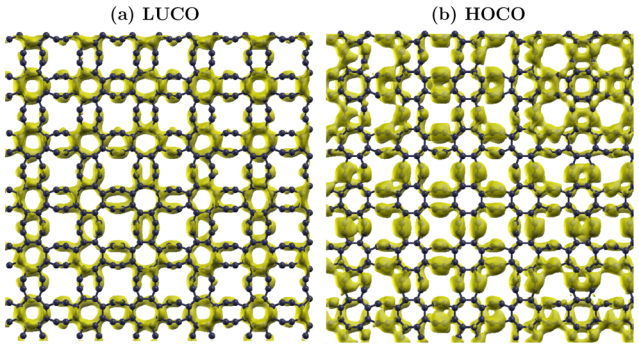


**Figure 7.** Spatial distribution for the (a) LUCO and (b) HOCO.

**Mechanical Properties.** Figure 8 presents the stress−strain curve for the uniaxial tensile loading in the $x$-direction.

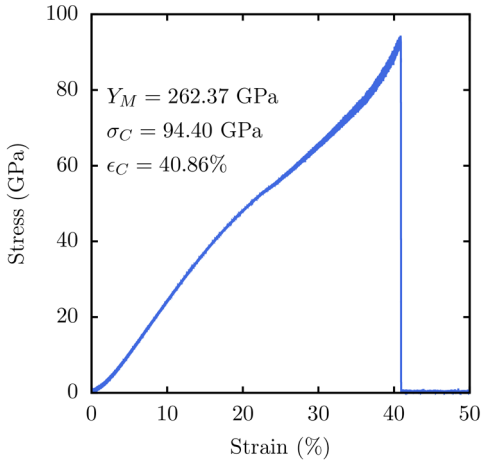


**Figure 8.** Stress−strain curve for S-GY as a function of the uniaxial applied strain along the $x$-direction.

Due to the symmetric nature of the S-GY lattice along the $x$- and $y$-directions, its mechanical properties are isotropic.

S-GY demonstrates a nearly linear elastic region when exposed to strain values up to 40%. Beyond this point, it suddenly transitions into a fractured configuration, characterized by zero stress, after reaching a critical strain ($\epsilon_C$) of 40.86%, as shown in Figure 8. The ultimate stress represents the tensile stress corresponding to the critical strain. The ultimate stress value ($\sigma_C$) for S-GY is 94.40 GPa, which is significantly lower than that of graphene (approximately 228.72 GPa[62]).

For calculating Young's modulus ($Y_M$), we considered a stress of 2%, resulting in a value of 262.37 GPa (or 87.6 N/m if we assume a structure thickness of 3.34 Å) for S-GY. This value is significantly lower than that of graphene and other similar 2D carbon-based structures.[62,63] Specifically, when comparing S-GY's Young's modulus with those of other graphyne structures, it is approximately half that of $\gamma$-graphyne, the same as that of $\beta$-graphyne, and twice that of $\alpha$-graphyne.[64] These differences can be attributed to the high porosity of S-GY.

We also obtained the stress−strain curve for DFT calculations up to 8% of strain (see the Supporting Information) to compare with the MD predictions. It is essential to acknowledge that the differences between DFT and MD predictions stem from the inherent nature of these approaches. Classical reactive MD simulations heavily rely on the chosen interatomic potential to describe atomic interactions, which can significantly impact the accuracy of predictions. Mortazavi and colleagues have implemented machine-learning interatomic potentials to address the limitations associated with this dependency.[65−68] Here, we opted for the widely used AIREBO potential, which has demonstrated reasonable accuracy in various systems. Furthermore, we aimed to illustrate the fracture patterns in the S-GY structure under uniaxial tensile strain, making classical reactive MD appropriate for this purpose.

We also examined the fracture patterns and dynamics of S-GY. Figures 9a−9f present several representative MD snapshots that capture critical moments in the stress dynamics. The color scheme indicates the von Mises stress per atom along the structure, which offers valuable insights into the fracture dynamics.[62]

Figure 9a represents the S-GY structure at 0.0% strain, while Figure 9b depicts it at 15.0% strain. Remarkably, the structural integrity of S-GY remains intact up to a strain of 35%, as shown in Figure 9c. However, beyond this critical point, at 40.90% strain (as depicted in Figure 9d), the lattice experiences the first bond breakage. Subsequently, an abrupt, brittlelike fracture occurs with rapid and linear crack propagation along the perpendicular direction of the stretch at 40.91% strain (see Figure 9e). This process leads to the separation of the S-GY lattice into two parts, connected by linear atomic chains (LACs), at 40.93% strain, as illustrated in Figure 9f. The fracture initiation starts from the acetylene bonds. For a more comprehensive understanding of this process, refer to video 1 in the Supporting Information.

**Melting Point.** The melting point analysis was conducted using a heating ramp protocol. Figure 10 displays the variation of total energy (black curve) and heat capacity ($C_V$, shown in blue) as a function of temperature. The total energy exhibits a quasi-linear increase within the temperature range of 300−2100 K, followed by a quasi-parabolic behavior from 2100 to





https://doi.org/10.1021/acs.jpcc.3c01788
J. Phys. Chem. C 2023, 127, 12226−12234

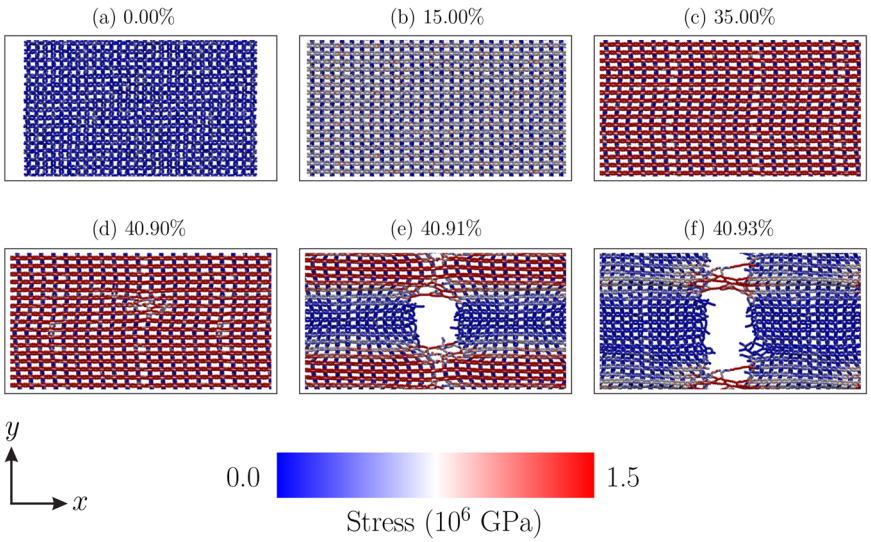


**Figure 9.** Representative MD snapshots for the S-GY subjected to a strain applied along the *x*-direction.

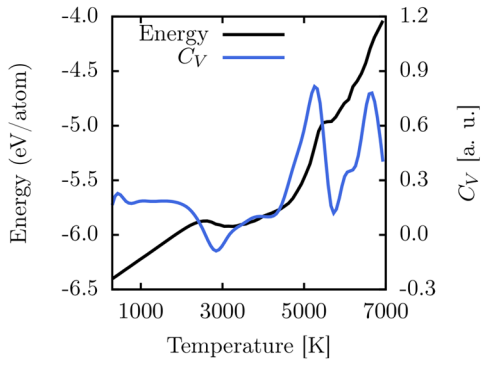


**Figure 10.** Total energy (black) and heat capacity ($C_V$, blue) values as a function of temperature for the S-GY monolayer.

5500 K. Subsequently, the total energy shows another quasi-linear increase for temperatures ranging from 5500 to 7000 K.

The most prominent peak in the $C_V$ curve corresponds to a melting point of approximately 2800 K (refer to Figure 10). During the initial stage of heating (300−2100 K), the S-GY lattice remains intact. However, at 2800 K, the thermal vibrations induce structural changes, leading to the melting process during the second heating stage (2100−5500 K). It is worth noting that the melting point of S-GY (2800 K) is lower than that of monolayer graphene (4095 K),[69] monolayer amorphous carbon (3626 K),[62] and biphenylene network (4024 K).[63] The final stage of the heating process (5500−7000 K), characterized by a significant change in the slope of the total energy curve, corresponds to the complete structural disintegration of S-GY, leading to its conversion into a gas phase.

Lastly, Figure 11 displays illustrative MD snapshots from the heating ramp simulation of S-GY, covering temperatures ranging from 2100 to 7000 K. In Figure 11a, the influence of thermal vibrations becomes evident as it induces alterations

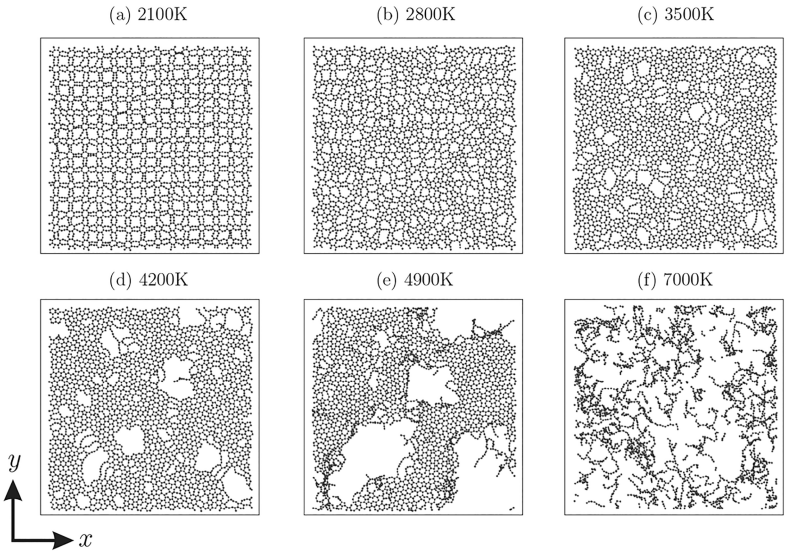


**Figure 11.** Representative MD snapshots for the heating ramp simulations (melting process) for S-GY at (a) 2100, (b) 2800, (c) 4200, (d) 4900, (e) 4000, and (f) 7000 K.



https://doi.org/10.1021/acs.jpcc.3c01788
J. Phys. Chem. C 2023, 127, 12226−12234

in the lattice morphology, resulting in numerous C−C bond breakages and reconstructions. Nevertheless, the general structural configuration remains comparable to the S-GY topology. Complete amorphization of the lattice transpires at 2800 K, as depicted in Figure 11b.

In the temperature range of 3500−5000 K, we note the emergence of graphene-like domains within the S-GY structure. These domains consist of lattice fragments composed of six-membered rings, as depicted in Figures 11c−11e. As the temperature surpasses 5000 K, the entire lattice undergoes complete atomization, rendering it into a gaseous phase, as demonstrated in Figure 11f. This process can be comprehensively understood by referring to video 2 in the Supporting Information.

## CONCLUSIONS

We comprehensively investigated the mechanical, structural, electronic, and optical properties of a 2D carbon allotrope here called Sun-Graphyne (S-GY), specifically the 8-16-4 graphyne structure. S-GY is characterized by an intriguing arrangement of carbon atoms, featuring two eight-atom carbon rings within its all-carbon structure. Our study employed a combination of DFT calculations and reactive MD simulations.

To assess the thermal and structural stability of S-GY, we performed AIMD simulations. The results confirm that S-GY exhibits remarkable stability, maintaining its structural morphology up to 1000 K. Furthermore, the DFT formation energy of S-GY was found to be −8.57 eV/atom, comparable to that of graphene (−8.8 eV/atom). These findings provide strong evidence supporting the structural stability of S-GY.

Electronic structure calculations have provided insights into the unique properties of S-GY, revealing it to be a semimetal material with a narrow band gap of approximately 5 meV. Notably, its electronic band structure exhibits two Dirac cones and manifests isotropic transport channels. These Dirac cones signify that the electrons in S-GY behave as massless Dirac fermions, similar to the behavior observed in graphene.

A striking characteristic of S-GY is its electronic band structure, which is unaltered even under moderate strain regimes. This exceptional stability of the electronic band structure under strain is a distinct feature of S-GY among 2D carbon allotropes. Unlike similar carbon-based materials with Dirac cones, S-GY does not undergo symmetry inversion under strain.

S-GY exhibits isotropic optical properties within the plane. Its reflectivity is predominantly confined to the infrared region and progressively diminishes to nearly zero as photon energies exceed 3 eV. The incident light on its surface is almost entirely absorbed, indicating its high transparency.

Regarding mechanical properties, S-GY exhibits a quasi-linear elastic region for strain values up to 40%. Beyond this point, it undergoes an abrupt transition to a fractured state, characterized by null stress, at a critical strain of 40.86%. The ultimate stress value and Young's modulus for S-GY are measured at 94.40 and 262.37 GPa, respectively. These values are significantly smaller than those of graphene[62] but comparable to other known graphyne structures.[64] These values are also considerably lower than those of similar 2D carbon-based structures, which can be attributed to the inherent porosity of S-GY.

The melting point of S-GY is lower than that of monolayer graphene (4095 K),[69] monolayer amorphous carbon (3626 K),[62] and biphenylene network (4024 K).[63] As the temperature increases between 3500 and 5000 K, the S-GY melting process tends to form graphene-like domains.

Given the recent advancements in graphyne synthesis, S-GY showcases distinct properties and holds potential for synthesis. We hope this study can stimulate further studies for this remarkable new structure.

## ASSOCIATED CONTENT

### Supporting Information

The Supporting Information is available free of charge at https://pubs.acs.org/doi/10.1021/acs.jpcc.3c01788.

Molecular dynamics video of the S-Gy fracture process (MPG)

Molecular dynamics video of the S-Gy melting process (MPG)

S-GY electronic band structure and related DOS for the unstrained case; stress−strain relationship of S-GY under uniaxial strain applied in the *x*-direction (PDF)

## AUTHOR INFORMATION


### Corresponding Author

**Luiz. A. Ribeiro Junior** − *University of Brasília,, Institute of Physics, Brasília, DF 70910-970, Brazil;* orcid.org/0000-0001-7468-2946; Email: ribeirojr@unb.br

### Authors

**Raphael M. Tromer** − *Applied Physics Department, State University of Campinas, Campinas, SP 13083-970, Brazil; Center for Computing in Engineering & Sciences, Unicamp, Campinas, SP 13083-970, Brazil*

**Marcelo L. Pereira Júnior** − *University of Brasília,, Faculty of Technology, Department of Electrical Engineering, Brasília 70910-970, Brazil*

**Kleuton A. L. Lima** − *Department of Physics, Federal University of Rio Grande do Norte, Natal, Rio Grande do Norte 59078-970, Brazil*

**Alexandre F. Fonseca** − *Applied Physics Department, State University of Campinas, Campinas, SP 13083-970, Brazil;* orcid.org/0000-0001-8413-9744

**Luciano R. da Silva** − *Department of Physics, Federal University of Rio Grande do Norte, Natal, Rio Grande do Norte 59078-970, Brazil; National Institute of Science and Technology for Complex Systems, Centro Brasileiro de Pesquisas Fisicas, Rio de Janeiro 22290-180, Brazil*

**Douglas S. Galvão** − *Applied Physics Department, State University of Campinas, Campinas, SP 13083-970, Brazil; Center for Computing in Engineering & Sciences, Unicamp, Campinas, SP 13083-970, Brazil;* orcid.org/0000-0003-0145-8358

Complete contact information is available at: https://pubs.acs.org/10.1021/acs.jpcc.3c01788


### Notes

The authors declare no competing financial interest.

## ACKNOWLEDGMENTS

This work was financed by the Coordenação de Aperfeiçoamento de Pessoal de Nível Superior (CAPES)-Finance Code 001 and grant 88887.691997/2022-00, Conselho Nacional de Desenvolvimento Científico e Tecnológico (CNPq), FAP-DF, and FAPESP. We thank the Center for Computing in Engineering and Sciences at Unicamp for financial support

through the FAPESP/CEPID Grants #2013/08293-7 and #2018/11352-7. A.F.F. acknowledges grants #303284/2021-8 from the Brazilian Agency CNPq and #2020/02044-9 from São Paulo Research Foundation (FAPESP). L.A.R.J acknowledges the financial support from FAP-DF grants 00193-00000857/2021-14, 00193-00000853/2021-28, 00193-00000811/2021-97, and, 00193.00001808/2022-71, CNPq grants 302922/2021-0 and 350176/2022-1, and FAPDF-PRONEM grant 00193.00001247/2021-20. L.A.R.J. gratefully acknowledges the support from ABIN grant 08/2019. L.R.d.S. acknowledges the National Institute of Science and Technology of Complex Systems (Brazil). L.A.R.J. acknowledges Núcleo de Computação de Alto Desempenho (NACAD) and for providing the computational facilities. This work used resources of the Centro Nacional de Processamento de Alto Desempenho em São Paulo (CENAPAD-SP). The authors acknowledge the National Laboratory for Scientific Computing (LNCC/MCTI, Brazil) for providing HPC resources of the SDumont supercomputer, contributing to the research results reported within this paper. URL: http://sdumont.lncc.br.

## REFERENCES

(1) Novoselov, K. S.; Geim, A. K.; Morozov, S. V.; Jiang, D.-e.; Zhang, Y.; Dubonos, S. V.; Grigorieva, I. V.; Firsov, A. A. Electric field effect in atomically thin carbon films. *science* **2004**, *306*, 666−669.
(2) Ando, T. The electronic properties of graphene and carbon nanotubes. *NPG Asia Materials* **2009**, *1*, 17−21.
(3) Sangwan, V. K.; Hersam, M. C. Electronic Transport in Two-Dimensional Materials. *Annu. Rev. Phys. Chem.* **2018**, *69*, 299−325.
(4) Song, H.; Liu, J.; Liu, B.; Wu, J.; Cheng, H.-M.; Kang, F. Two-Dimensional Materials for Thermal Management Applications. *Joule* **2018**, *2*, 442−463.
(5) Kumar, R.; Joanni, E.; Singh, R. K.; Singh, D. P.; Moshkalev, S. A. Recent advances in the synthesis and modification of carbon-based 2D materials for application in energy conversion and storage. *Prog. Energy Combust. Sci.* **2018**, *67*, 115−157.
(6) Lu, H.; Li, S.-D. Two-dimensional carbon allotropes from graphene to graphyne. *Journal of Materials Chemistry C* **2013**, *1*, 3677−3680.
(7) Wang, Z.; Dong, F.; Shen, B.; Zhang, R.; Zheng, Y.; Chen, L.; Wang, S.; Wang, C.; Ho, K.; Fan, Y.-J.; et al. Electronic and optical properties of novel carbon allotropes. *Carbon* **2016**, *101*, 77−85.
(8) Enyashin, A. N.; Ivanovskii, A. L. Graphene allotropes. *physica status solidi (b)* **2011**, *248*, 1879−1883.
(9) Wang, Z.; Zhou, X.-F.; Zhang, X.; Zhu, Q.; Dong, H.; Zhao, M.; Oganov, A. R. Phagraphene: a low-energy graphene allotrope composed of 5−6−7 carbon rings with distorted dirac cones. *Nano Lett.* **2015**, *15*, 6182−6186.
(10) Wang, S.; Yang, B.; Chen, H.; Ruckenstein, E. Popgraphene: a new 2D planar carbon allotrope composed of 5−8−5 carbon rings for high-performance lithium-ion battery anodes from bottom-up programming. *Journal of Materials Chemistry A* **2018**, *6*, 6815−6821.
(11) Zhuo, Z.; Wu, X.; Yang, J. Me-graphene: a graphene allotrope with near zero Poisson's ratio, sizeable band gap, and high carrier mobility. *Nanoscale* **2020**, *12*, 19359−19366.
(12) Karaush, N. N.; Baryshnikov, G. V.; Minaev, B. F. DFT characterization of a new possible graphene allotrope. *Chem. Phys. Lett.* **2014**, *612*, 229−233.
(13) Zhang, R.-S.; Jiang, J.-W. The art of designing carbon allotropes. *Front. Phys.* **2019**, *14*, 1−17.
(14) Berber, S.; Osawa, E.; Tománek, D. Rigid crystalline phases of polymerized fullerenes. *Phys. Rev. B* **2004**, *70*, 085417.
(15) Alsayoud, A. Q.; Manga, V. R.; Muralidharan, K.; Vita, J.; Bringuier, S.; Runge, K.; Deymier, P. Atomistic insights into the effect of polymerization on the thermophysical properties of 2-D C60 molecular solids. *Carbon* **2018**, *133*, 267−274.
(16) Tromer, R. M.; Machado, L. D.; Woellner, C. F.; Galvao, D. S. Thiophene-Tetrathia-Annulene monolayer (TTA-2D): A new 2D semiconductor material with indirect bandgap. *Physica E: Low-dimensional Systems and Nanostructures* **2021**, *129*, 114586.
(17) Tromer, R. M.; Felix, I. M.; Freitas, A.; Azevedo, S.; Pereira, L. F. C. Diboron-porphyrin monolayer: A new 2D semiconductor. *Comput. Mater. Sci.* **2020**, *172*, 109338.
(18) Jana, S.; Bandyopadhyay, A.; Datta, S.; Bhattacharya, D.; Jana, D. Emerging properties of carbon based 2D material beyond graphene. *J. Phys.: Condens. Matter* **2022**, *34*, 053001.
(19) Toh, C.-T.; Zhang, H.; Lin, J.; Mayorov, A. S.; Wang, Y.-P.; Orofeo, C. M.; Ferry, D. B.; Andersen, H.; Kakenov, N.; Guo, Z.; et al. Synthesis and properties of free-standing monolayer amorphous carbon. *Nature* **2020**, *577*, 199−203.
(20) Fan, Q.; Yan, L.; Tripp, M. W.; Krejčí, O.; Dimosthenous, S.; Kachel, S. R.; Chen, M.; Foster, A. S.; Koert, U.; Liljeroth, P.; et al. Biphenylene network: A nonbenzenoid carbon allotrope. *Science* **2021**, *372*, 852−856.
(21) Desyatkin, V. G.; Martin, W. B.; Aliev, A. E.; Chapman, N. E.; Fonseca, A. F.; Galvão, D. S.; Miller, E. R.; Stone, K. H.; Wang, Z.; Zakhidov, D.; Limpoco, F. T.; Almahdali, S. R.; Parker, S. M.; Baughman, R. H.; Rodionov, V. O. Scalable Synthesis and Characterization of Multilayer γ-Graphyne, New Carbon Crystals with a Small Direct Band Gap. *J. Am. Chem. Soc.* **2022**, *144*, 17999−18008.
(22) Hou, L.; Cui, X.; Guan, B.; Wang, S.; Li, R.; Liu, Y.; Zhu, D.; Zheng, J. Synthesis of a monolayer fullerene network. *Nature* **2022**, *606*, 507−510.
(23) Baughman, R. H.; Eckhardt, H.; Kertesz, M. Structure-property predictions for new planar forms of carbon: Layered phases containing sp2 and sp atoms. *J. Chem. Phys.* **1987**, *87*, 6687−6699.
(24) Coluci, V.; Braga, S.; Legoas, S.; Galvao, D.; Baughman, R. Families of carbon nanotubes: Graphyne-based nanotubes. *Phys. Rev. B* **2003**, *68*, 035430.
(25) Baughman, R. H.; Galvao, D. S. Crystalline networks with unusual predicted mechanical and thermal properties. *Nature* **1993**, *365*, 735−737.
(26) Solis, D. A.; Borges, D. D.; Woellner, C. F.; Galvao, D. S. Structural and thermal stability of graphyne and graphdiyne nanoscroll structures. *ACS Appl. Mater. Interfaces* **2019**, *11*, 2670−2676.
(27) Liu, S.; Wang, H.; Ma, F.; Du, H.; Liu, B. Two-dimensional carbon materials with an anisotropic Dirac cone: high stability and tunable Fermi velocity. *Phys. Chem. Chem. Phys.* **2022**, *24*, 19263−19268.
(28) Zhang, W.; Chai, C.; Fan, Q.; Song, Y.; Liu, Y.; Yang, Y.; Sun, M.; Schwingenschlögl, U. Semimetallic 2D Alkynyl Carbon Materials with Distorted Type I Dirac Cones. *J. Phys. Chem. C* **2021**, *125*, 18022−18030.
(29) Adjizian, J.-J.; Briddon, P.; Humbert, B.; Duvail, J.-L.; Wagner, P.; Adda, C.; Ewels, C. Dirac Cones in two-dimensional conjugated polymer networks. *Nat. Commun.* **2014**, *5*, 5842.
(30) Chen, X.; Bouhon, A.; Li, L.; Peeters, F. M.; Sanyal, B. PAI-graphene: A new topological semimetallic two-dimensional carbon allotrope with highly tunable anisotropic Dirac cones. *Carbon* **2020**, *170*, 477−486.
(31) Bandyopadhyay, A.; Datta, S.; Jana, D.; Nath, S.; Uddin, M. M. The topology and robustness of two Dirac cones in S-graphene: A tight binding approach. *Sci. Rep.* **2020**, *10*, 2502.
(32) Wang, G.; Si, M.; Kumar, A.; Pandey, R. Strain engineering of Dirac cones in graphyne. *Appl. Phys. Lett.* **2014**, *104*, 213107.
(33) Bandyopadhyay, A.; Majumdar, A.; Chowdhury, S.; Ahuja, R.; Jana, D. 8−16−4 graphyne: Square-lattice two-dimensional nodal line semimetal with a nontrivial topological Zak index. *Phys. Rev. B* **2021**, *103*, 075137.
(34) Kang, J.; Wei, Z.; Li, J. Graphyne and Its Family: Recent Theoretical Advances. *ACS Appl. Mater. Interfaces* **2019**, *11*, 2692−2706.




https://doi.org/10.1021/acs.jpcc.3c01788
J. Phys. Chem. C 2023, 127, 12226−12234

(35) Desyatkin, V. G.; Martin, W. B.; Aliev, A. E.; Chapman, N. E.; Fonseca, A. F.; Galvão, D. S.; Miller, E. R.; Stone, K. H.; Wang, Z.; Zakhidov, D.; Limpoco, F. T.; Almahdali, S. R.; Parker, S. M.; Baughman, R. H.; Rodionov, V. O. Scalable Synthesis and Characterization of Multilayer γ-Graphyne, New Carbon Crystals with a Small Direct Band Gap. *J. Am. Chem. Soc.* **2022**, *144*, 17999−18008.
(36) Lundgren, C.; Kakanakova-Georgieva, A.; Gueorguiev, G. K. A perspective on thermal stability and mechanical properties of 2D Indium Bismide from ab initio molecular dynamics. *Nanotechnology* **2022**, *33*, 335706.
(37) Sangiovanni, D. G.; Faccio, R.; Gueorguiev, G. K.; Kakanakova-Georgieva, A. Discovering atomistic pathways for supply of metal atoms from methyl-based precursors to graphene surface. *Phys. Chem. Chem. Phys.* **2022**, *25*, 829−837.
(38) dos Santos, R. B.; Rivelino, R.; Gueorguiev, G. K.; Kakanakova-Georgieva, A. Exploring 2D structures of indium oxide of different stoichiometry. *CrystEngComm* **2021**, *23*, 6661−6667.
(39) Sheng, X.-L.; Cui, H.-J.; Ye, F.; Yan, Q.-B.; Zheng, Q.-R.; Su, G. Octagraphene as a versatile carbon atomic sheet for novel nanotubes, unconventional fullerenes, and hydrogen storage. *J. Appl. Phys.* **2012**, *112*, 074315.
(40) Farooq, F. B. Topological properties of nano sheets based on octa graphene. *Journal of Mathematics* **2022**, *2022*, 1−9.
(41) Jana, S.; Bandyopadhyay, A.; Jana, D. Acetylenic linkage dependent electronic and optical behaviour of morphologically distinct '-ynes'. *Phys. Chem. Chem. Phys.* **2019**, *21*, 13795−13808.
(42) Soler, J. M.; Artacho, E.; Gale, J. D.; García, A.; Junquera, J.; Ordejón, P.; Sánchez-Portal, D. The SIESTA method for ab initio order-N materials simulation. *J. Phys.: Condens. Matter* **2002**, *14*, 2745.
(43) Perdew, J. P.; Burke, K.; Ernzerhof, M. Generalized Gradient Approximation Made Simple. *Phys. Rev. Lett.* **1996**, *77*, 3865−3868.
(44) Ernzerhof, M.; Scuseria, G. E. Assessment of the Perdew−Burke−Ernzerhof exchange-correlation functional. *J. Chem. Phys.* **1999**, *110*, 5029−5036.
(45) Troullier, N.; Martins, J. L. Efficient pseudopotentials for plane-wave calculations. *Phys. Rev. B* **1991**, *43*, 1993−2006.
(46) Dion, M.; Rydberg, H.; Schröder, E.; Langreth, D. C.; Lundqvist, B. I. Van der Waals Density Functional for General Geometries. *Phys. Rev. Lett.* **2004**, *92*, 246401.
(47) Thonhauser, T.; Cooper, V. R.; Li, S.; Puzder, A.; Hyldgaard, P.; Langreth, D. C. Van der Waals density functional: Self-consistent potential and the nature of the van der Waals bond. *Phys. Rev. B* **2007**, *76*, 125112.
(48) Román-Pérez, G.; Soler, J. M. Efficient Implementation of a van der Waals Density Functional: Application to Double-Wall Carbon Nanotubes. *Phys. Rev. Lett.* **2009**, *103*, 096102.
(49) Evans, D. J.; Holian, B. L. The Nose−Hoover thermostat. *J. Chem. Phys.* **1985**, *83*, 4069−4074.
(50) Tromer, R. M.; da Luz, M. G. E.; Ferreira, M. S.; Pereira, L. F. C. Atomic Adsorption on Nitrogenated Holey Graphene. *J. Phys. Chem. C* **2017**, *121*, 3055−3061.
(51) Thompson, A. P.; Aktulga, H. M.; Berger, R.; Bolintineanu, D. S.; Brown, W. M.; Crozier, P. S.; in't Veld, P. J.; Kohlmeyer, A.; Moore, S. G.; Nguyen, T. D.; et al. LAMMPS-a flexible simulation tool for particle-based materials modeling at the atomic, meso, and continuum scales. *Comput. Phys. Commun.* **2022**, *271*, 108171.
(52) Plimpton, S. Fast Parallel Algorithms for Short-Range Molecular Dynamics. *J. Comput. Phys.* **1995**, *117*, 1−19.
(53) Stuart, S. J.; Tutein, A. B.; Harrison, J. A. A reactive potential for hydrocarbons with intermolecular interactions. *J. Chem. Phys.* **2000**, *112*, 6472−6486.
(54) Hoover, W. G. Canonical dynamics: equilibrium phase-space distributions. *Phys. Rev. A* **1985**, *31*, 1695.
(55) Humphrey, W.; Dalke, A.; Schulten, K. VMD: Visual molecular dynamics. *J. Mol. Graphics* **1996**, *14*, 33−38.
(56) Heimann, R. B.; Evsvukov, S. E.; Koga, Y. Carbon allotropes: a suggested classification scheme based on valence orbital hybridization. *Carbon* **1997**, *35*, 1654−1658.
(57) Enyashin, A. N.; Ivanovskii, A. L. Graphene allotropes. *physica status solidi (b)* **2011**, *248*, 1879−1883.
(58) Wang, X.-Q.; Li, H.-D.; Wang, J.-T. Structural stabilities and electronic properties of planar C4 carbon sheet and nanoribbons. *Phys. Chem. Chem. Phys.* **2012**, *14*, 11107−11111.
(59) Tromer, R. M.; Freitas, A.; Felix, I. M.; Mortazavi, B.; Machado, L. D.; Azevedo, S.; Pereira, L. F. C. Electronic, optical and thermoelectric properties of boron-doped nitrogenated holey graphene. *Phys. Chem. Chem. Phys.* **2020**, *22*, 21147−21157.
(60) Hu, Y.; Wu, C.; Pan, Q.; Jin, Y.; Lyu, R.; Martinez, V.; Huang, S.; Wu, J.; Wayment, L. J.; Clark, N. A.; et al. Synthesis of γ-graphyne using dynamic covalent chemistry. *Nature Synthesis* **2022**, *1*, 449−454.
(61) Barua, M.; Saraswat, A.; Rao, C. A novel method for synthesis of γ-graphyne and their charge transfer properties. *Carbon* **2022**, *200*, 247−252.
(62) Felix, L. C.; Tromer, R. M.; Autreto, P. A.; Ribeiro Junior, L. A.; Galvao, D. S. On the mechanical properties and thermal stability of a recently synthesized monolayer amorphous carbon. *J. Phys. Chem. C* **2020**, *124*, 14855−14860.
(63) Pereira, M.; da Cunha, W.; de Sousa, R.; Nze, G. D. A.; Galvão, D.; Ribeiro, L. On the mechanical properties and fracture patterns of the nonbenzenoid carbon allotrope (biphenylene network): a reactive molecular dynamics study. *Nanoscale* **2022**, *14*, 3200−3211.
(64) Kanegae, G. B.; Fonseca, A. F. Effective acetylene length dependence of the elastic properties of different kinds of graphynes. *Carbon Trends* **2022**, *7*, 100152.
(65) Mortazavi, B.; Podryabinkin, E. V.; Roche, S.; Rabczuk, T.; Zhuang, X.; Shapeev, A. V. Machine-learning interatomic potentials enable first-principles multiscale modeling of lattice thermal conductivity in graphene/borophene heterostructures. *Materials Horizons* **2020**, *7*, 2359−2367.
(66) Mortazavi, B.; Zhuang, X. Low and anisotropic tensile strength and thermal conductivity in the single-layer fullerene network predicted by machine-learning interatomic potentials. *Coatings* **2022**, *12*, 1171.
(67) Mortazavi, B.; Silani, M.; Podryabinkin, E. V.; Rabczuk, T.; Zhuang, X.; Shapeev, A. V. First-principles multiscale modeling of mechanical properties in graphene/borophene heterostructures empowered by machine-learning interatomic potentials. *Adv. Mater.* **2021**, *33*, 2102807.
(68) Mortazavi, B.; Podryabinkin, E. V.; Novikov, I. S.; Roche, S.; Rabczuk, T.; Zhuang, X.; Shapeev, A. V. Efficient machine-learning based interatomic potentialsfor exploring thermal conductivity in two-dimensional materials. *Journal of Physics: Materials* **2020**, *3*, 02LT02.
(69) Los, J.; Zakharchenko, K.; Katsnelson, M.; Fasolino, A. Melting temperature of graphene. *Phys. Rev. B* **2015**, *91*, 045415.




https://doi.org/10.1021/acs.jpcc.3c01788
J. Phys. Chem. C 2023, 127, 12226−12234